ChemComm

COMMUNICATION

View Article Online
View Journal

Cite this: DOI: 10.1039/d5cc02372f

Received 28th April 2025,
Accepted 26th August 2025

DOI: 10.1039/d5cc02372f

rsc.li/chemcomm

Developing a Zn(II)-metallovesicle for loading and delivering doxorubicin to kill cancer cells—a multi-drug delivery system

Abhishek Dutta, Subhajit Ghosh and Parthasarathi Dastidar *

An amphiphilic Zn(II)-coordination polymer (CP3) was rationally designed, successfully synthesised, and crystallographically characterized. It was derived from the non-steroidal anti-inflammatory drug (NSAID) flurbiprofen, as well as isophthalic acid and $Zn(NO_3)_2$. CP3 was loaded with the anti-cancer drug doxorubicin, which was delivered to multicellular spheroids of the HeLa cancer cells, thereby making it suitable for developing a multi-drug delivery system.

Among the various supramolecular entities, vesicles are one of the most important classes of supramolecular structures because they play significant roles in biology, biomedical applications, such as drug delivery and therapeutics, and material science. A vesicle is a spherical structure composed of single or multiple layers of a supramolecular membrane that holds liquid at its core. Vesicles are ubiquitous in biology—a biological cell itself is a vesicular structure enclosing cytoplasm and various organelles within a phospholipid bilayer cell membrane. It is understandable that a living cell would not survive without a cell membrane because it provides protection against various biological and chemical attacks, allows essential nutrients to diffuse in and wastes to diffuse out, and plays key roles in processes such as exocytosis and endocytosis.

Scientists have drawn inspiration from the intriguing structure and function of the cell membrane and attempted to create a synthetic mimic. Soon after the first report of a synthetic multi-layered vesicle by Kunitake *et al.*,[1] many synthetic vesicles were developed from organic and inorganic molecules.[2–10] However, there have been difficulties due to the complexities involved in multi-step organic synthesis, the cytotoxicity associated with organic precursors, and the challenges associated with the loading of drugs and their release at the target site, and multi-drug loading for combination therapy.

Supramolecular systems derived from metal–organic precursors[11–18] are being vigorously studied because of the fact that they are relatively easy to synthesize and are amenable to synthetic modulation directed by atomic level insights through single crystal X-ray diffraction (SXRD) studies. Furthermore, they also offer opportunities to incorporate more than one drug (*e.g.*, active pharmaceutical ingredients) for combination therapy. One drug molecule can act as a ligand of the metal–organic precursors, and another drug molecule can be encapsulated within the core of the supramolecular system (vesicle).

Combination therapy (delivering more than one drug) has become important in drug delivery research.[19–21] The process has been found to be quite effective because it appears to elude cellular resistance through optimal performance of each drug *via* different key signal transduction pathways.[22–25] Such synergistic effects of drugs are beneficial because they may enable reduced dosages and side effects.[26–28]

The key to designing metallovesicles is to synthesize amphiphilic 1D coordination polymer chains, wherein a hydrophobic drug and/or its derivative can be anchored to the metal center of the 1D chains formed due to extended coordination of a suitable bidentate ligand with a metal center. Such an amphiphilic coordination polymer chain is expected to self-assemble in aqueous solvent to form metallovesicles, which can easily encapsulate another drug (*e.g.*, an anti-cancer drug), thereby making it a potential multi-drug delivery system (Scheme 1). The reaction of two pyridyl derivatives of ibuprofen and flurbiprofen (3-pyIBU and 4-pyFLR, respectively) with two bidentate ligands, namely di-sodium terephthalate (Na_2TA), and di-sodium isophthalate (Na_2IA) and $Zn(NO_3)_2$, readily produced crystalline products, namely $[\{(3\text{-pyIBU})_2Zn(\mu\text{-TA})0.5(\mu\text{-TA})0.5\}.0.5MeOH]_\infty$ (**CP1**), $[\{(3\text{-pyIBU})_2Zn(\mu\text{-IA})_2(MeOH)\}\cdot H_2O]_\infty$ (**CP2**), and $[\{(IA)(H_2O)(4\text{-pyFLR})(Zn_1)(\mu\text{-IA})(Zn_2)(H_2O)(DMF)(4\text{-pyFLR})\}\cdot(2H_2O)\ (DMF)]_\infty$ (**CP3**) (Scheme 2), as revealed by SXRD (*vide infra*).

The close connection between inflammation and cancer[29,30] prompted us to incorporate the non-steroidal anti-inflammatory drug (NSAID) derivatives 3-pyIBU and 4-pyFLR (synthesized using a previously reported procedure[31]) in the metal–organic precursor as one of the drug molecules in the multi-drug delivery system that we set out to develop. A redshift of the carboxylates in the

School of Chemical Science, Indian Association for the Cultivation of Science (IACS), 2a, 2b Raja S. C. Mullick Road, Kolkata 700032, West Bengal, India. E-mail: ocpd@iacs.res.in, ocpdastidar@gmail.com

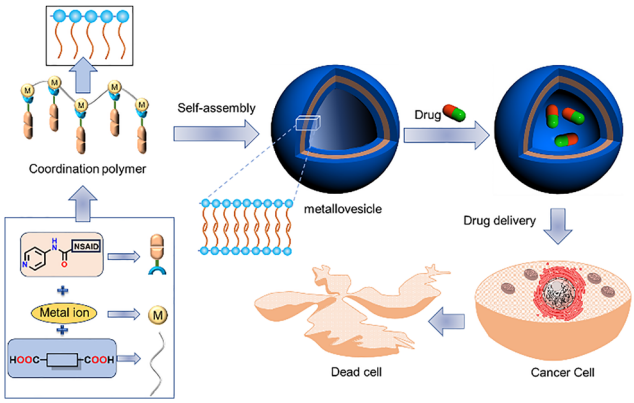

Scheme 1 Designing a metallovesicle for multi-drug delivery.

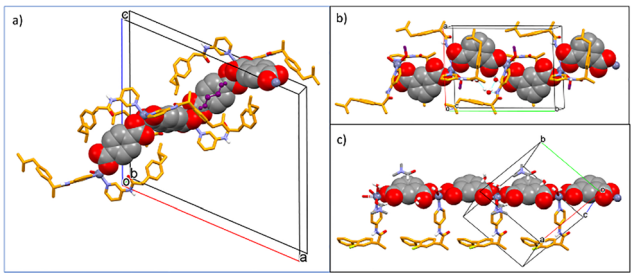

Fig. 1 Crystal structure illustrations of (a) **CP1**, (b) **CP2**, and (c) **CP3**. (IA and TA moieties are shown in a space-filling model; carbon atoms of 4-pyFLR and 3-pyIBU are shown in orange; coordinated and lattice-occluded methanol are shown in magenta; solvate water and DMF are shown in a capped stick model).

FT-IR spectra (1583–1691 to 1549–1610 cm^{-1}) of all the coordination polymers indicated strong metal-carboxylate coordination (Fig. S8 and Table S1, SI).

Single crystals of **CP1–CP3** were subjected to SXRD (Table S2, SI). Crystal structure analyses revealed that **CP1** and **CP2** displayed similar structural features. Monoclinic crystals of **CP1** and **CP2** (space groups *C*2/*c* and $P2_1/c$, respectively) showed distorted tetrahedral and square pyramidal Zn(II) coordination geometry, respectively. The coordination sites of Zn(II) in **CP1** were occupied by two 3-pyIBU and two TA. In **CP2**, the axial position of the square pyramidal Zn(II) was occupied by a MeOH molecule, and the equatorial sites were coordinated by two 3-pyIBU and two IA. In both cases, extended coordination with Zn(II) through the carboxylates produced 1D coordination polymer chain, wherein each metal center was coordinated by two 3-pyIBU molecules. The 1D chains were packed in a parallel fashion sustained by various hydrogen bonding involving the amide and carboxylate moieties, and lattice-occluded solvent molecules (MeOH and H_2O, respectively).

Interestingly, there were two crystallographically independent Zn(II) metal centres displaying distorted tetrahedral (Zn1) and octahedral (Zn2) coordination geometry in **CP3** (triclinic, $P\bar{1}$). The coordination sphere of the tetrahedral Zn1 was coordinated by two carboxylates (IA), one 4-pyFLR, and one water molecule, whereas that of octahedral Zn2 was ligated by two IA, one 4-pyFLR, one DMF, and one water molecule. Extended coordination through IA resulted in a 1D coordination polymer chain, wherein Zn1 and Zn2 were placed in an alternating fashion (Fig. 1).

As envisaged, single crystal structures of **CP1–CP3** displayed 1D polymer chains, wherein the hydrophobic NSAID moieties were anchored to the metal centres. Intriguingly, in **CP3**, only one NSAID moiety per metal centre was present, as compared to two in **CP1** and **CP2**. Moreover, the 4-pyFLR moieties in **CP3** were oriented in the same direction, thereby demarcating clear hydrophobic and hydrophilic (metal centres coordinated to water, DMF, and carboxylates) zones, suggesting the amphiphilic character of **CP3**.

Dilute suspensions (1 mg mL^{-1} in 5% DMSO/water) of **CP3** under FEG-TEM clearly displayed spherical morphology (approximately 90 nm), whereas **CP1** and **CP2** showed aggregates of nanoparticles. The spherical morphology of the same suspension of **CP3** was also evident in FE-SEM and AFM. Interestingly, the height profile of the AFM images (100–150 nm diameter *vis-à-vis* a height of 6–10 nm) indicated that the vesicular structure was most likely flattened due to drying of the sample (Fig. 2 and Fig. S13, SI).

The data suggested that the amphiphilic **CP3** was capable of self-assembling to assume a vesicular structure in aqueous medium. To confirm this further, dynamic light scattering (DLS) experiments using the same suspension of **CP3** were conducted. Accumulation of particles having a hydrodynamic diameter $D_h = 120 \pm 30$ nm with a narrow size distribution over a period of 60 days further supported the formation of vesicular aggregates. The concentration-dependent DLS data showed that the vesicular aggregates disintegrated into small particles upon dilution below a concentration of 0.25 mg mL^{-1}. The percent intensity of the vesicular particles ($D_h = 120 \pm 30$ nm) did not follow the trend (*i.e.*, slow increase with time) for the 'blackberry' vesicular structure observed for some metal–organic polyhedra (Fig. S14 and S15, SI).[32–34]

The foregoing data suggested that the amphiphilic 1D coordination polymer chain of **CP3** plausibly self-assembled to form a lamellae architecture in polar solvent as any amphiphilic molecule would do, and further folded to produce a vesicular structure having a hydrophilic core (Scheme 3).

To assess the accessibility of the hydrophilic core of the **CP3**-vesicle, **CP3** (1.0 mg) and the highly fluorescent dye calcein (0.2 mg) were suspended in a snake-skin dialysis bag

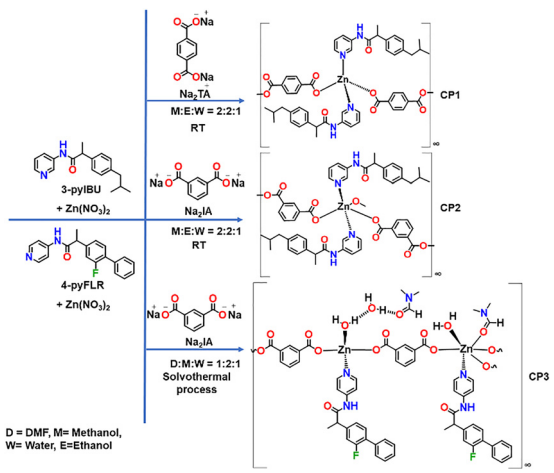

Scheme 2 Synthesis of the coordination polymers reported herein.

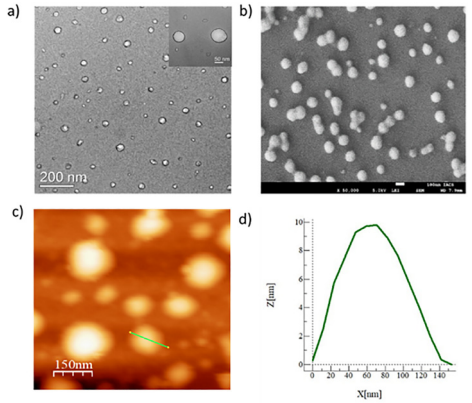

Fig. 2 Images of metallovesicles derived from **CP3** suspensions. (a) TEM image (scale bar = 200 nm) (enlarged TEM image in inset), (b) SEM image (scale bar = 100 nm), (c) AFM image (scale bar = 150 nm), (d) height profile of AFM image of the selected green-marked vesicle.

containing 5% DMSO/water (2 mL) and dialyzed four times, for 72 h each time, against 5% DMSO/water. A bathochromic shift (7 nm) of the λ_{max} of free calcein from 486 nm to 493 nm for the content of the dialysis bag clearly suggested that the dye experienced a confined environment that implied encapsulation of calcein within the hydrophilic core of the **CP3**-vesicle. Significant quenching of the emission of calcein (λ_{em} = 515 nm, λ_{ex} = 450 nm) in the aliquots of the content of the dialysis bag clearly supported the formation of **CP3**-vesicles that could encapsulate calcein. Interestingly, the green fluorescence of calcein in **CP3**-vesicle@calcein under a fluorescence microscope was also observed. The loading efficiency of the dye within the **CP3**-vesicle was found to be 7.5%.

Similar experiments with the anti-cancer drug doxorubicin (DOX) displayed a significant bathochromic shift of 23 nm for free DOX (λ_{max} = 480 nm) *vis-à-vis* **CP3**-vesicle@DOX (λ_{max} = 503 nm), indicating entrapment of DOX within the hydrophilic core of the **CP3**-vesicle, with a loading efficiency of 3% (0.8 μg mL^{-1}). Emission of DOX was significantly quenched in **CP3**-vesicle@DOX, similar to that observed for calcein. Interestingly, red fluorescence of **CP3**-vesicle@DOX was observed by fluorescence microscopy (Fig. S16 and S17, SI). The data presented thus far clearly establishes that the amphiphilic **CP3** successfully formed vesicles, and the hydrophilic core of which was accessible for drug loading.

The cytotoxicity of **CP3**-vesicle@DOX against human embryonic kidney (HEK 293) cells was 250 μg mL^{-1} (IC_{50}) with no such haemolytic activity, whereas more than 50% of human cervical carcinoma cells (HeLa) could be killed at a much lower concentration (60–125 μg mL^{-1}) (Fig. S18 and S19, SI). The multi-drug combination effect of **CP3**-vesicle@DOX was also assessed using CompuSyn software,[36] and the results validated the synergistic effect from **CP3** and DOX (Fig. S18 and S20, SI).

We performed a drug release experiment at pH 7.4 (PBS), and found that DOX was not released to the media (Fig. S21). Interestingly, when we performed the same experiment at pH 5.4, we observed a significant release of DOX to the media with time (up to 24 h) (Fig. S21). This is intriguing because the results indicate that the drug is released at a lower pH, *i.e.*, under acidic conditions. The ability of **CP3**-vesicle@DOX to kill cancer cells indicates that it is first internalized and then releases the drug at a low pH, likely in the lysosome.

To confirm that, and show colocalization of fluorescence of **CP3**-vesicle@DOX (red fluorescence of DOX), we carried out experiments with LysoTracker™ Green using confocal microscopy on HeLa cells. Fig. S21 clearly shows the colocalization of red and green fluorescence (yellow). The images clearly establish that **CP3**-vesicle@DOX was internalized and released DOX through the lysosome.

The delivery of DOX from **CP3**-vesicle@DOX to HeLa cells was also demonstrated by a cell migration assay.[35] It quantified the speed of migration of cancer cells in the presence of a potential anti-cancer agent. The slower the speed, the greater the efficiency of the anti-cancer agent. It was observed that the migration speed (22 μm h^{-1}) during control experiments was significantly reduced (2 μm h^{-1}) in treated cells with **CP3**-vesicle@DOX. Although the **CP3**-vesicle and DOX also reduced the speed (10 μm h^{-1} and 11 μm h^{-1}, respectively) of cell migration, it was not as low as 2 μm h^{-1}, indicating the successful and synergistic effect of **CP3**-vesicle@DOX (Fig. 3).

A growth-delay experiment was performed on a 3D multicellular spheroid generated from HeLa cells treated with **CP3**-vesicle@DOX (0.1 mg mL^{-1} in water), **CP3** vesicles (0.1 mg mL^{-1} in 5% DMSO-water), and DOX (0.4 μg mL^{-1} in water) and compared with that of untreated cells. It was clear from the images that the size of the spheroids gradually increased in non-treated cells, whereas significant inhibition of growth of the spheroids was observed in treated cells. This demonstrated that **CP3**-vesicle@DOX was also significantly active against multicellular spheroids of HeLa cancer cells (Fig. 4 and Fig. S22, SI).

The results presented in this study clearly demonstrate that an amphiphilic coordination polymer, **CP3**, could indeed be accessed through rational design and synthesis. The formation of **CP3**-vesicles was established through various experiments (TEM, SEM, AFM, DLS), which corroborated well with the structural features revealed by the SXRD of **CP3**. The ability of **CP3**-vesicle@DOX to kill cancer cells (HeLa) *in vitro* (MTT, scratch assay) and multicellular spheroids was also demonstrated. Thus, formation of metallovesicles (**CP3**-vesicle) containing an NSAID derivative (4-pyFLR) as a part of the metal–organic system and its ability to load and deliver the anti-cancer drug DOX to HeLa cells clearly demonstrated that **CP3**-vesicle@DOX can indeed work as a multi-drug delivery system.

A. D. synthesized and characterized all the CPs. Biological studies were carried out by A. D. and S. G. under the supervision of S. G.; P. D. conceptualized and supervised the project, analysed the results, and co-wrote the manuscript with input from all the co-authors.

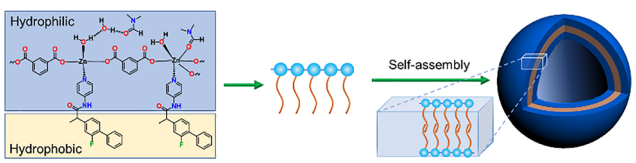

Scheme 3 Plausible model for metallovesicle formation using **CP3**.

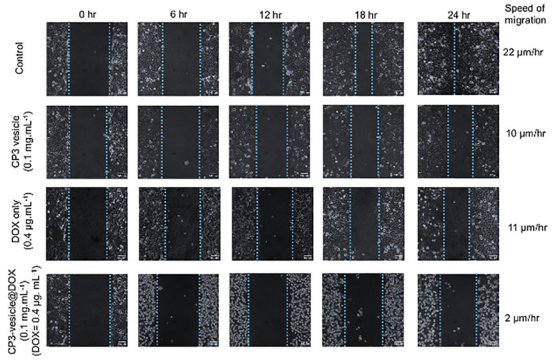

Fig. 3 Cell migration assay using HeLa cells (scale bar = 100 μm).

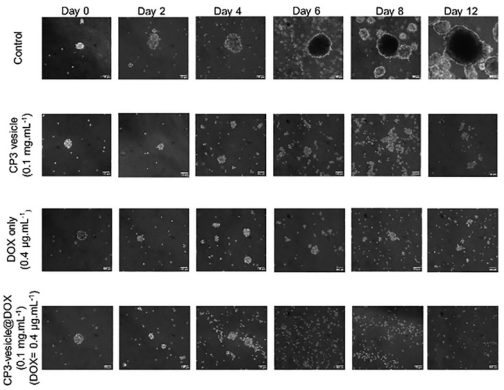

Fig. 4 Delivery of DOX by **CP3**-vesicle@DOX to multicellular spheroids of HeLa cells (scale bar = 100 μm).

P. D. thanks SERB (CRG/2023/001598) for the financial support. S. G. thanks SERB for RA-1, and A. D. thanks CSIR for SRF. A.D. thanks Mr Tathagata Bhattacharya for assisting in collecting fluorescence microscopy images.

Data availability

The data supporting this article have been included as part of the SI.

Supplementary Information: Experimental section, synthesis of the ligand and CPs, IR and NMR data, SXRD data analysis and tables, metallovesicle formation study and characterisation by DLS, biological and anticancer activity, hemolytic activity study, and CIFs. See DOI: **https://doi.org/10.1039/d5cc02372f**.

CCDC 2420262–2420264 contain the supplementary crystallographic data for this paper.[37a–c]

Conflicts of interest

There are no conflicts to declare.

Notes and references

1 T. Kunitake and Y. Okahata, *J. Am. Chem. Soc.*, 1977, **99**, 3860–3861.
2 J. Voskuhl and B. J. Ravoo, *Chem. Soc. Rev.*, 2009, **38**, 495.
3 W. Jiang, Y. Zhou and D. Yan, *Chem. Soc. Rev.*, 2015, **44**, 3874.
4 N. Sakai and S. Matile, *Nat. Chem.*, 2009, **1**, 599.
5 M. J. Webber and R. Langer, *Chem. Soc. Rev.*, 2017, **46**, 6600.
6 F. M. Menger and M. I. Angelova, *Acc. Chem. Res.*, 1998, **31**, 789.
7 C. Li, S. Zhang, J. Pang, Y. Wu and Z. Gu, *Adv. Funct. Mater.*, 2015, **25**, 3764.
8 H. Oh, A. M. Ketner, R. Heymann, E. Kesselman, D. Danino, D. E. Falvey and S. R. Raghavan, *Soft Matter*, 2013, **9**, 5025–5033.
9 P. Zhu, L. Z. Zhou, Y. Y. Song, L. Cai, M. H. Ji, J. Wang, G. Ruan and J. Chen, *J. Mater. Chem. B*, 2020, **8**, 4899–4907.
10 E. N. Savariar, S. V. Aathimanikandan and S. Thayumanavan, *J. Am. Chem. Soc.*, 2006, **128**, 16224–16230.
11 S. Rojas, A. Arenas-vivo and P. Horcajada, *Coord. Chem. Rev.*, 2019, **388**, 202–226.
12 N. Giri and S. L. James, *Chem. Commun.*, 2011, **47**, 1458–1460.
13 F. M. Menger, L. H. Gan, E. Johnson and D. H. Durst, *J. Am. Chem. Soc.*, 1987, **109**, 2800–2803.
14 S. Bera, A. Chowdhury, K. Sarkar and P. Dastidar, *Chem. – Asian J.*, 2020, **15**, 503–510.
15 H. T. Baytekin, B. Baytekin, A. Schulz and C. A. Schalley, *Small*, 2009, **5**, 194–197.
16 D. Li, J. Zhang, K. Landskron and T. Liu, *J. Am. Chem. Soc.*, 2008, **130**, 4226–4227.
17 D. Li, W. Zhou, K. Landskron, S. Sato, C. J. Kiely, M. Fujita and T. Liu, *Angew. Chem., Int. Ed.*, 2011, **50**, 5182–5187.
18 P. Biswas, K. Sarkar and P. Dastidar, *Macromol. Biosci.*, 2020, **20**, 2000044.
19 F. Greco and M. J. Vicent, *Adv. Drug Delivery Rev.*, 2009, **61**, 1203–1213.
20 K. A. Parato, D. Senger, P. A. J. Forsyth and J. C. Bell, *Nat. Rev. Cancer*, 2005, **5**, 965–976.
21 A. Casadevall, E. Dadachova and L. A. Pirofski, *Nat. Rev. Microbiol.*, 2004, **2**, 695–703.
22 J. S. Logue and D. K. Morrison, *Genes Dev.*, 2012, **26**, 641–650.
23 V. Fodale, M. Pierobon, L. Liotta and E. Petricoin, *Cancer J.*, 2011, **17**, 89–95.
24 V. S. Goldmacher, T. Chittenden, R. V. J. Chari, Y. V. Kovtun and J. M. Lambert in *Annual Reports in Medicinal Chemistry*, ed. J. E. Macor, Elsevier, Waltham, 2012, vol. 23, pp. 349–357.
25 H. Zhang, G. Wang and H. Yang, *Expert Opin. Drug Delivery*, 2011, **8**, 171–190.
26 D. Conway and J. A. Cohen, *Lancet Neurol.*, 2010, **9**, 299–308.
27 M. Chowers, B. S. Gottesman, L. Leibovici, J. M. Schapiro and M. Paul, *Eur. J. Clin. Microbiol. Infect. Dis.*, 2010, **29**, 779–786.
28 A. M. Jacobine, J. R. Mazzone, R. D. Slack, A. K. Tripathi, D. J. Sullivan and G. H. Posner, *J. Med. Chem.*, 2012, **55**, 7892–7899.
29 F. Balkwill and A. Mantovani, *Lancet*, 2001, **357**, 539–545.
30 K. Wakabayashi, *Asian Pac. J. Cancer Prev.*, 2000, **1**, 97–113.
31 P. Biswas and P. Dastidar, *Chem. Commun.*, 2022, **58**, 969–972.
32 D. Li, J. Zhang, K. Landskron and T. Liu, *J. Am. Chem. Soc.*, 2008, **130**, 4226–4227.
33 D. Li, W. Zhou, K. Landskron, S. Sato, C. J. Kiely, M. Fujita and T. Liu, *Angew. Chem., Int. Ed.*, 2011, **50**, 5182–5187.
34 K. Sarkar, M. Paul and P. Dastidar, *Chem. Commun.*, 2016, **52**, 13124–13127.
35 J. Deb, J. Majumder, S. Bhattacharyya and S. S. Jana, *BMC Cancer*, 2014, **14**, 567.
36 N. Zhang, J. N. Fu and T. C. Chou, *Am. J. Cancer Res.*, 2015, **6**, 97–104.
37 (*a*) A. Dutta, S. Ghosh and P. Dastidar, CCDC 2420262: Experimental Crystal Structure Determination, 2025, DOI: **10.5517/ccdc.csd.cc2m7gzb**; (*b*) A. Dutta, S. Ghosh and P. Dastidar, CCDC 2420263: Experimental Crystal Structure Determination, 2025, DOI: **10.5517/ccdc.csd.cc2m7h0d**; (*c*) A. Dutta, S. Ghosh and P. Dastidar, CCDC 2420264: Experimental Crystal Structure Determination, 2025, DOI: **10.5517/ccdc.csd.cc2m7h1f**.

